Transition Metal Chemistry (2018) 43:171–183
https://doi.org/10.1007/s11243-018-0205-9

# Oxovanadium phenanthroimidazole derivatives: synthesis, DNA binding and antitumor activities

Yin-Liang Bai[1] · Ya-Wu Zhang[2] · Ji-Yuan Xiao[1] · Hai-Wei Guo[3] · Xiang-Wen Liao[3] · Wen-Jie Li[4] · You-Cheng Zhang[2]

Received: 28 September 2017 / Accepted: 5 January 2018 / Published online: 24 January 2018


**Abstract**
Four unsymmetrical oxovanadium phenanthroimidazole complexes, [VO(hntdtsc)(NPIP)] (**1**), [VO(hntdtsc)(CPIP)] (**2**), [VO(hntdtsc)(MEPIP)] (**3**) and [VO(hntdtsc)(HPIP)] (**4**) (hntdtsc = 2-hydroxy-1-naphthaldehyde thiosemicarbazone, NPIP = 2-(4-nitrophenyl)-imidazo[4,5-f]1,10-phenanthroline, CPIP = 2-(4-chlorphenyl)-imidazo[4,5-f]1,10-phenanthroline), MEPIP = 2-(4-methylphenyl)-imidazo[4,5-f]1,10-phenanthroline), HPIP = 2-(4-hydroxylphenyl)-imidazo[4,5-f] 1,10-phenanthroline), have been synthesized and characterized. Their DNA binding and antitumor activities were determined by biochemical methods. All four oxovanadium complexes can bind with CT-DNA by an intercalation model and can also cleave supercoiled plasmid DNA in the presence of $H_2O_2$. The antitumor properties and mechanism of the complexes have been analyzed by MTT assay, cell cycle analysis, apoptosis assay and Western blot analysis. The results showed that the free ligands and their corresponding complexes all possess antiproliferative activities with very low $IC_{50}$ values against Hela, BIU-87 and SPC-A-1 cell lines. Complex **1**, which has a strongly electron-withdrawing nitro group, exhibited the best antiproliferative activities. Complex **1** caused $G_0/G_1$ phase arrest of the cell cycle and induced apoptosis in Hela cells. Additionally, complex **1** attenuated the phosphorylation of extracellular signal-regulated kinases 1 and 2 (ERK1/2).This indicates that inhibition of the ERK1/2 signaling pathway may contribute to the antitumor effects of these complexes.

## Introduction

Vanadium has attracted considerable attention, because its complexes with organic ligands can possess a variety of biological functions such as antibacterial, antitumor, insulin-enhancing and antiparasitic effects [1–6]. Vanadium complexes have been investigated in tumor therapy due to their considerable antiproliferation role in certain cancers [7–9]. The general mechanisms for antitumor action by vanadium complexes involve inhibition of DNA repair processes [10], opening of mitochondrial permeability transition pores, subsequent release of cytochrome c, resulting in cancer cell apoptosis [11, 12]. In addition, vanadium compounds can enhance uptake of redox-active essential metal ions, primarily Cu(II), from extracellular media into cells, causing disruption of cellular thiol levels. Vanadium complexes can also have insulin-mimetic and antidiabetic properties by increasing the cellular uptake of glucose by the GLUT4 transporter [13].

In previous work, it was found that vanadium complexes of thiosemicarbazones and 1,10-phenanthroline ligands can possess excellent antiproliferative activities. Organic ligands, especially with aromatic substituents, can enhance their biological activities [14]. In this paper, we report the preparation of four new oxovanadium complexes of thiosemicarbazones, namely 2-(4-nitrophenyl)-imidazo[4,5-f]1,10-phenanthroline (NPIP), 2-(4-chlorphenyl)-imidazo[4,5-f]1,10-phenanthroline (CPIP), 2-(4-methylphenyl)-imidazo[4,5-f]1,10-phenanthroline (MEPIP) and 2-(4-hydroxylphenyl)-imidazo[4,5-f]1,10-phenanthroline (HPIP), together with an investigation of their antitumor activities. NPIP and CPIP possess strongly electron-withdrawing groups, while MEPIP and HPIP possess electron-donating groups.

✉ You-Cheng Zhang
lzuzhangych@163.com

[1] Department of Pharmacy, Lanzhou University Second Hospital, Lanzhou 730030, China

[2] Department of General Surgery, Lanzhou University Second Hospital, Cuiying Men Road 82, Lanzhou 730030, China

[3] School of Pharmacy, Guangdong Pharmaceutical University, Guangzhou 510006, China

[4] Department of Clinical Pharmacology, School of Pharmaceutical Sciences, Zhengzhou University, Zhengzhou 450001, China

Oxovanadium complexes of these ligands, [VO(hntdtsc)(NPIP)] (**1**), [VO(hntdtsc)(CPIP)] (**2**), [VO(hntdtsc)(MEPIP)] (**3**) and [VO(hntdtsc)(HPIP)] (**4**), were prepared and fully characterized by elemental analysis, UV–Vis, MS, IR and NMR. The interactions of these complexes with calf-thymus DNA (CT-DNA) were investigated by UV–Vis and fluorescence spectroscopy, and by viscosity measurements. Their cleavage reactions with pBR322 supercoiled plasmid DNA were studied by gel electrophoresis. In addition, their antitumor properties and mechanism of action have been analyzed by MTT assay, cell cycle analysis, apoptosis assay and Western blot analysis. The results showed that the free ligands and their corresponding complexes all possess antitumor activities with very low $IC_{50}$ values and complex **1** exhibited the highest activity against tumor cells.

## Results and discussion

### Synthesis and characterization

[VO(hntdtsc)(NPIP)] (**1**), [VO(hntdtsc)(CPIP)] (**2**), [VO(hntdtsc)(MEPIP)] (**3**) and [VO(hntdtsc)(HPIP)] (**4**) were prepared by refluxing hntdtsc and vo(acac)$_2$ with NPIP, CPIP, MEPIP and HPIP, respectively, in absolute methanol. Elemental analysis, MS, IR and NMR spectroscopy were implemented to characterize the complexes and the free ligands. The structures of these complexes and free ligands are shown in Scheme 1.

The IR spectra show peaks from the Schiff bases(–NH–) at 3450–3160 $cm^{-1}$, aromatic (C–H) at 2987–3050 $cm^{-1}$, azomethine group (–CH=N) and (C=C) at 1592–1626 $cm^{-1}$. The position of the azomethine peak was reduced in frequency compared the corresponding free ligands, consistent with coordination of the azomethine nitrogen to vanadium. The strong VO signal could also be clearly identified at 945–955 $cm^{-1}$ [14]. In their ES-MS spectra, the free ligands showed molecular peaks of *m/z* 246.0 ($[M + 1]^+$) (hntdtsc), 342.0 ($[M + 1]^+$) (NPIP), 331.1 ($[M + 1]^+$) (CPIP), 327.1 ($[M + 1]^+$) (MEPIP) and 313.0 ($[M + 1]^+$) (HPIP). The oxovanadium complexes gave molecular peaks at *m/z* 652.1 ($[M + 1]^+$) (**1**), 639.1 ($[M + 1]^+$) (**2**), 619.1 ($[M + 1]^+$) (**3**) and 623.0 ($[M + 1]^+$) (**4**).

In the $^1$H and $^{13}$C-NMR spectra of the free ligands recorded in DMSO-$d_6$, all the protons due to heteroaromatic groups were found in their expected regions. In addition, for the four complexes, the peaks of hydroxyl (OH), amine ($NH_2$) and (NHCO) were absent, indicating that these ligand groups were coordinated to vanadium.

### DNA-binding studies

#### Absorption titrations

Absorption titrations in the UV–Vis range were carried out in order to investigate the interactions of these complexes with CT-DNA. Hypochromism and bathochromism can occur with the intercalation of complexes into the base pairs of DNA [15, 16], which is correlated with the stacking interactions between the planar aromatic chromophore of the complexes and the base pairs of DNA. For metal interaction, DNA binding is associated with hypochromism and showed a redshift in the MLCT and ligand bands.

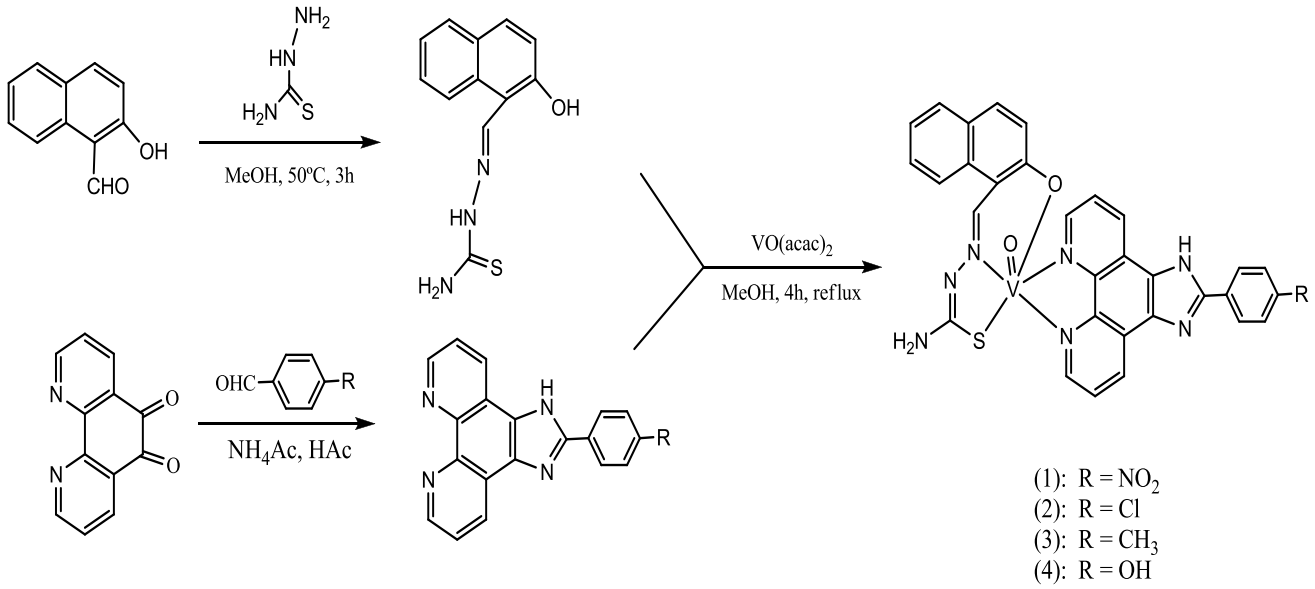


**Scheme 1** Structure of the ligands and complexes

Figure 1 shows the electronic spectra of the four oxovanadium complexes obtained in the presence of CT-DNA. Appreciable hypochromism and bathochromism can be observed for all four complexes with increasing amounts of DNA. The specific values of hypochromism and bathochromism were 41.6% and 3.5 nm (complex **1**), 38.8% and 2.5 nm (complex **2**), 32.4% and 2 nm (complex **3**), 31.3% and 2 nm (complex **4**). In addition, the intrinsic binding constant $K_b$ was calculated by monitoring the change in absorbance with increasing amounts of CT-DNA; the $K_b$ values of complexes **1**, **2**, **3** and **4** were $1.53 \times 10^5$ $M^{-1}$, $1.41 \times 10^5$ $M^{-1}$, $1.05 \times 10^5$ $M^{-1}$ and $0.95 \times 10^5$ $M^{-1}$, respectively. Complex **1** has the highest $K_b$, and the values suggest that these oxovanadium complexes may bind to DNA in an intercalative mode.

### Fluorescence spectroscopic studies

Fluorescence spectroscopic titration experiments were performed in Tris buffer A. The emission spectra of the four complexes in the absence and presence of CT-DNA are shown in Fig. 2 and clearly increase the intensity of the luminescence emitted by the complexes steadily upon increasing the amount of CT-DNA, suggesting that these four oxovanadium complexes may intercalate into the base pairs of the DNA. The hydrophobic environment inside the DNA helix reduces the accessibility of water molecules to the complexes, thus lengthening their luminescence lifetimes and increasing their emission intensity [17–19].

### Viscosity measurements

In the absence of X-ray structure data, viscosity measurements, which are sensitive to the change in the length of DNA, are considered to be the most critical test of the classical intercalation model and provide the most definitive means of inferring the binding mode of DNA in solution. The viscosity of the DNA solution is expected to increase significantly if the intercalation mode is in operation, whereas partial, non-classical intercalation will have a small effect on the viscosity [20–25].

Figure 3 shows the effect of the complexes on the viscosity of CT-DNA. The viscosity is significantly increased with increasing complex concentration, in the order **1** > **2** > **3** > **4**. This result also supports an intercalation mode for the binding of all four complexes to DNA.

## DNA cleavage

To further elucidate the interaction of DNA with these complexes, DNA cleavage experiments were carried out in order to monitor the cleavage reaction on supercoiled plasmid DNA by agarose gel electrophoresis. When circular plasmid DNA is subject to electrophoresis, relatively fast migration will be observed for the intact supercoiled form (Form I). If scission occurs on one strand, the supercoil will relax to generate a slower moving open circular form (Form II) [26, 27].

The results of our experiments are shown in Figs. 4 and 5. No obvious cleavage of DNA was observed in the absence of any complex (lanes 11 and 12 in Figs. 4, 5, respectively). However, the open circular form (Form II) was observed in the presence of different concentrations of complexes **1**, **2**, **3** and **4** (Figs. 4, 5). Hence, all four complexes possess DNA cleavage ability. To explore the DNA cleavage mechanism, control experiments were carried out in the presence of L-histamine or dimethyl sulfoxide (DMSO). No significant change was observed in the presence of L-histamine, which is a singlet oxygen quencher. However, in the presence of the hydroxyl radical scavenger DMSO, inhibition of DNA cleavage occurred, suggesting that the •OH free radical is likely to be the reactive species for the cleavage reaction. This can be explained by the generation of •OH radicals obtained from the oxidation of $VO^{2+}$ in the presence of $H_2O_2$ [28].

## Antitumor activities

### Cytotoxicity assays

The complexes and the corresponding free ligands were evaluated for their ability to inhibit the growth of Hela, BIU-87 and SPC-A-1 cell lines using MTT assays [29, 30]. The $IC_{50}$ values were calculated after 24 h of incubation with the test compound at different concentrations using cisplatin as a control. The results are listed in Table 1. All four oxovanadium complexes as well as the free ligands showed significant cytotoxicities against all three tumor cells, and the antitumor activities were also concentration dependent. Complex **1** showed the largest inhibitory effects against the Hela, BIU-87 and SPC-A-1 cell lines with $IC_{50}$ values of $1.09 \pm 0.16$, $4.51 \pm 0.68$ and $7.61 \pm 0.55$ μM, respectively. Overall, the antitumor activities follow the order **1** > **2** > **3** > **4**, consistent with their DNA-binding abilities.

It should be noted that under the same conditions, the $IC_{50}$ of complex **1** was lower than that of cisplatin, which gave $IC_{50}$ values against the Hela, BIU-87 and SPC-A-1 cell lines of $5.54 \pm 0.81$, $7.82 \pm 0.64$ and $8.65 \pm 1.01$ μM, respectively. The potency of complex **1** and its high affinity for DNA may be associated with the presence of an electron-withdrawing nitro group in this complex.

### Cell cycle analysis

The cell cycle distribution was analyzed by flow cytometry with PI staining, in order to further elucidate the mechanism of the antiproliferative effect of these complexes on cancer cells. Hela cells were treated with complex **1** at different

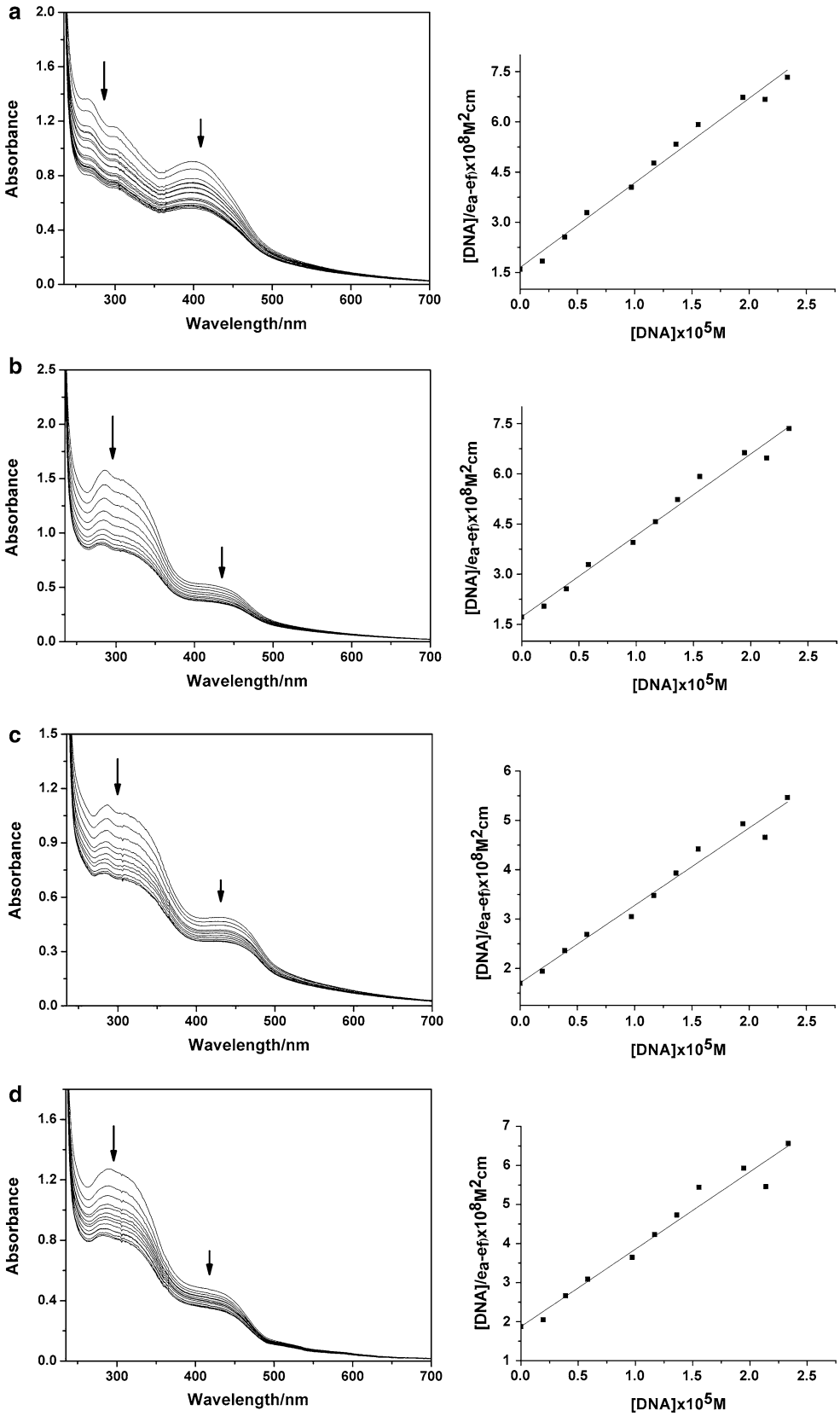


**Fig. 1** Absorption spectral trace of the complexes **1** (**a**), **2** (**b**), **3** (**c**) and **4** (**d**) on the addition of CT-DNA in Tris–HCl buffer A. $[V] = 20$ μM. Arrow shows the decreasing absorbance with the increasing amounts of CT-DNA. Plots of [DNA]/($\varepsilon_a - \varepsilon_f$) versus [DNA] for the titration of [*V*] with CT-DNA

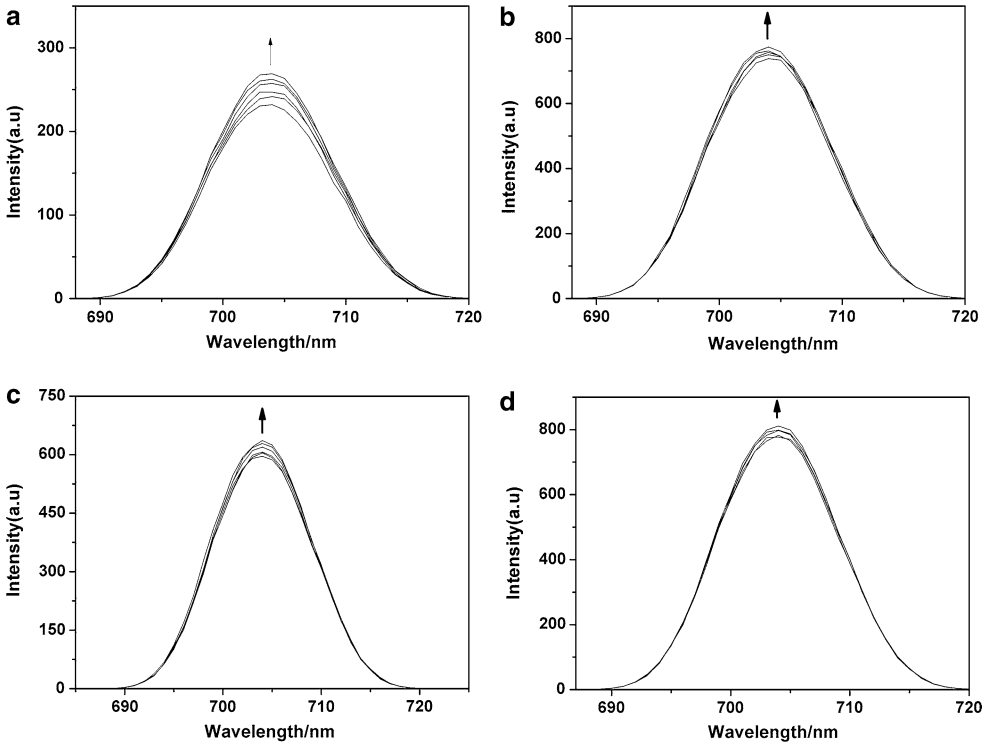


**Fig. 2** Emission spectra of complexes **1** (**a**), **2** (**b**), **3** (**c**) and **4** (**d**) in Tris–HCl buffer A in the absence and presence of CT-DNA. [*V*] = 20 μM. Arrows show the increasing intensity with the increasing concentration of DNA

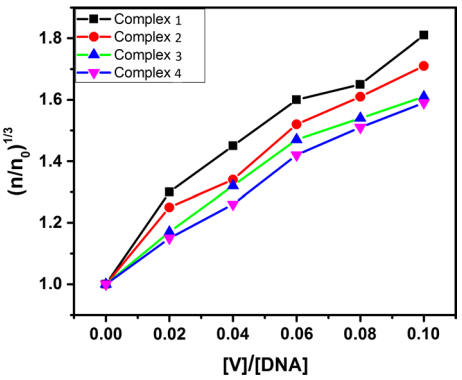


**Fig. 3** Effects of increasing amounts of complexes **1** (filled square), **2** (filled circle), **3** (filled triangle) and **4** (filled inverted triangle) on the relative viscosity of CT-DNA at 28(± 0.1) °C [DNA] = 0.40 mM

concentrations (0.5, 1.0 and 2.0 μM) for 24 h. This experiment significantly increased the proportion of cells at $G_0/G_1$ phase and decreased the proportion of cells at *S* and $G_2/M$ phases (Fig. 6). This indicates that the complex inhibits the growth of Hela cells by disrupting the $G_0/G_1$ phase of the cell cycle.

The occurrence of apoptosis was further investigated with Hoechst 33258 staining to investigate whether the inhibition of cell growth in the Hela cells caused by complex **1** was associated with apoptosis. Representative staining fluorescence photomicrographs of cultured Hela cells treated with or without complex **1** are shown in Fig. 7. As can be readily observed by comparison with the control, the cells treated with complex **1** exhibited typical apoptotic features after 24 h, including cellular

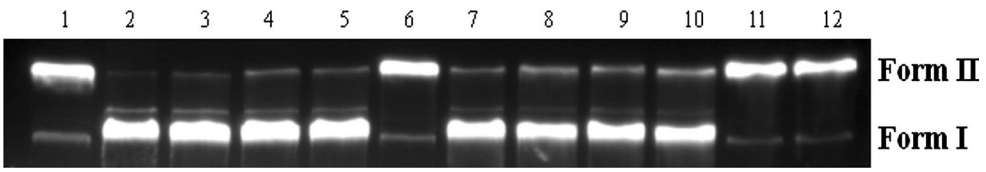


**Fig. 4** Cleavage of pBR322 DNA by oxidovanadium complexes **1** and **2** (15–60 μM) in the absence and presence of $H_2O_2$ (30 mM) in buffer B (pH 7.2). Lane 12, DNA control; lane 11, DNA + $H_2O_2$; lane 10, DNA + **1** (15 μM) + $H_2O_2$; lane 9, DNA + **1** (30 μM) + H2O2; lane 8, DNA + **1** (60 μM) + $H_2O_2$; lane 7, DNA + **1** (30 μM) + $H_2O_2$ + L-histidine (0.02 M); lane 6, DNA + **1** (30 μM) + $H_2O_2$ + DMSO (2 μL); lane 5, DNA + **2** (15 μM) + $H_2O_2$; lane **2**, DNA + **2** (30 μM) + $H_2O_2$; lane 3, DNA + **2** (60 μM) + $H_2O_2$; lane 2, DNA + **2** (30 μM) + $H_2O_2$ + L-histidine (0.02 M); lane 1, DNA + **2** (30 μM) + $H_2O_2$ + DMSO (2 μL)

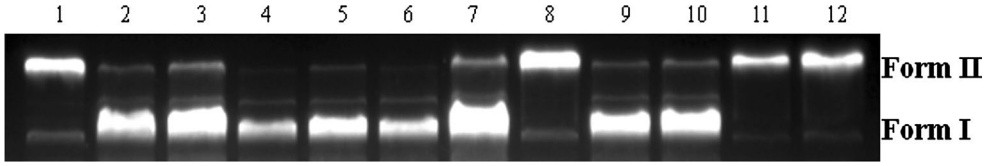


**Fig. 5** Cleavage of pBR322 DNA by oxidovanadium complexes **3** and **4** (15–60 μM) in the absence and presence of $H_2O_2$ (30 mM) in buffer B (pH 7.2). Lane 12, DNA control; lane 11, DNA + $H_2O_2$; lane 10, DNA + **3** (15 μM) + $H_2O_2$; lane 9, DNA + **3** (30 μM) + $H_2O_2$; lane 7, DNA + **3** (60 μM) + $H_2O_2$; lane 6, DNA + **3** (30 μM) + $H_2O_2$ + L-histidine (0.02 M); lane 8, DNA + **3** (30 μM) + $H_2O_2$ + DMSO (2 μL); lane 5, DNA + **4** (15 μM) + $H_2O_2$; lane **2**, DNA + **4** (30 μM) + $H_2O_2$; lane 3, DNA + **4** (60 μM) + $H_2O_2$; lane 2, DNA + **4** (30 μM) + $H_2O_2$ + L-histidine (0.02 M); lane 1, DNA + **4**(30 μM) + $H_2O_2$ + DMSO (2 μL)

**Table 1** The $IC_{50}$ values for complexes and ligands against Hela, BIU-87 and SPC-A-1 cell lines

| Compounds | IC50 (μM) | | |
|---|---|---|---|
| | Hela | BIU-87 | SPC-A-1 |
| Cisplatin | 5.54 ± 0.81 | 7.82 ± 0.64 | 8.65 ± 1.01 |
| hntdtsc | 100.04 ± 7.56 | 98.16 ± 6.78 | 74.56 ± 5.63 |
| $VO(acac)_2$ | 87.21 ± 7.24 | 76.87 ± 6.12 | 84.14 ± 5.89 |
| CPIP | 39.69 ± 7.12 | 60.23 ± 5.12 | 41.02 ± 3.45 |
| NPIP | 24.35 ± 1.63 | 39.65 ± 5.56 | 31.01 ± 5.01 |
| MEPIP | 41.02 ± 4.63 | 56.45 ± 7.36 | 61.02 ± 6.32 |
| HPIP | 78.62 ± 7.02 | 47.89 ± 4.12 | 54.36 ± 2.13 |
| VO(hntdtsc)CPIP | 10.36 ± 1.23 | 8.69 ± 1.05 | 21.43 ± 3.24 |
| VO(hntdtsc)NPIP | 1.09 ± 0.16 | 4.51 ± 0.68 | 7.61 ± 0.55 |
| VO(hntdtsc)MEPIP | 20.11 ± 2.68 | 34.52 ± 3.67 | 24.63 ± 4.37 |
| VO(hntdtsc)HPIP | 40.26 ± 4.01 | 19.86 ± 2.47 | 26.32 ± 4.75 |

The $IC_{50}$ values for complexes and ligands against Hela, BIU-87 and SPC-A-1 cell lines. All data were presented as mean ± SE

morphological change, fragmentation, apoptotic bodies, condensation of chromatin (brightly stained) and membrane blebbing. Furthermore, the proportion of apoptotic cells increased in a dose-dependent manner.

Annexin V-FITC/PI staining was implemented to determine early, late apoptotic and necrotic cells with the results shown in Fig. 8. The proportion of Annexin V-FITC-stained cells (both early and late apoptotic cells) increased with increasing concentrations of complex **1**; the proportions were 25.8% (0.5 μM), 53.9% (1.0 μM) and 81.4% (2.0 μM), respectively. Also, complex **1** was found to predominantly cause early apoptotic cells, such that the proportions of Annexin V-FITC-stained early apoptotic cells were 18.3% (0.5 μM), 47.5% (1.0 μM) and 75.2% (2.0 μM). In conclusion, the results suggest that complex **1** induces proliferative suppression of Hela cells predominantly via the induction of apoptosis.

### Phosphorylation of ERK1/2

As shown in Fig. 9, Western blot analysis showed that both complex **1** (2 μM) and U0126 (ERK inhibitor) attenuated the phosphorylation of ERK1/2 in Hela cells treated for 24 h ($P < 0.05$; $P < 0.05$, respectively). The total ERK1/2 levels were not significantly different among the groups.

## Conclusion

In this study, four oxovanadium complexes of mixed thiosemicarbazone and phenanthroimidazole ligands have been prepared and characterized. All four of the complexes can bind with CT-DNA by intercalation and also show efficient cleavage of supercoiled plasmid DNA in the presence of $H_2O_2$. Both the free ligands and their corresponding complexes all possess cytotoxic activities against Hela, BIU-87 and SPC-A-1 cell lines, and complex **1** exhibited the highest activity against tumor cells. The proliferative suppression of Hela cells by complex **1** is predominantly via the induction of apoptosis and inhibition of tumor cell growth by inducing a block in the $G_0/G_1$ phase of the cell cycle. Complex **1** which has an electron-withdrawing nitro substituent and larger DNA-binding affinity also exhibited highest cytotoxic activity against tumor cells; taken together with the results of a previous study [14], this suggests that the introduction of electron-withdrawing groups to phenanthroimidazole ligands may enhance the biological activity of their vanadium complexes.

Mitogen-activated protein kinase (MAPK) cascades are key signaling pathways involved in the regulation of cell proliferation, apoptosis, survival and differentiation. Aberrant regulation of MAPK cascades can contribute to cancer. In particular, the extracellular signal-regulated kinase (ERK), as one of MAPKs subtypes, is widely involved in human oncogenesis [45–47]. ERK is a downstream component of the Ras–Raf–MEK–ERK–MAPK signaling pathway. Activated Raf phosphorylates and activates the kinase MEK, which in turn phosphorylates and activates ERK kinase. Activated ERK regulates a number of cellular events, including cell cycle

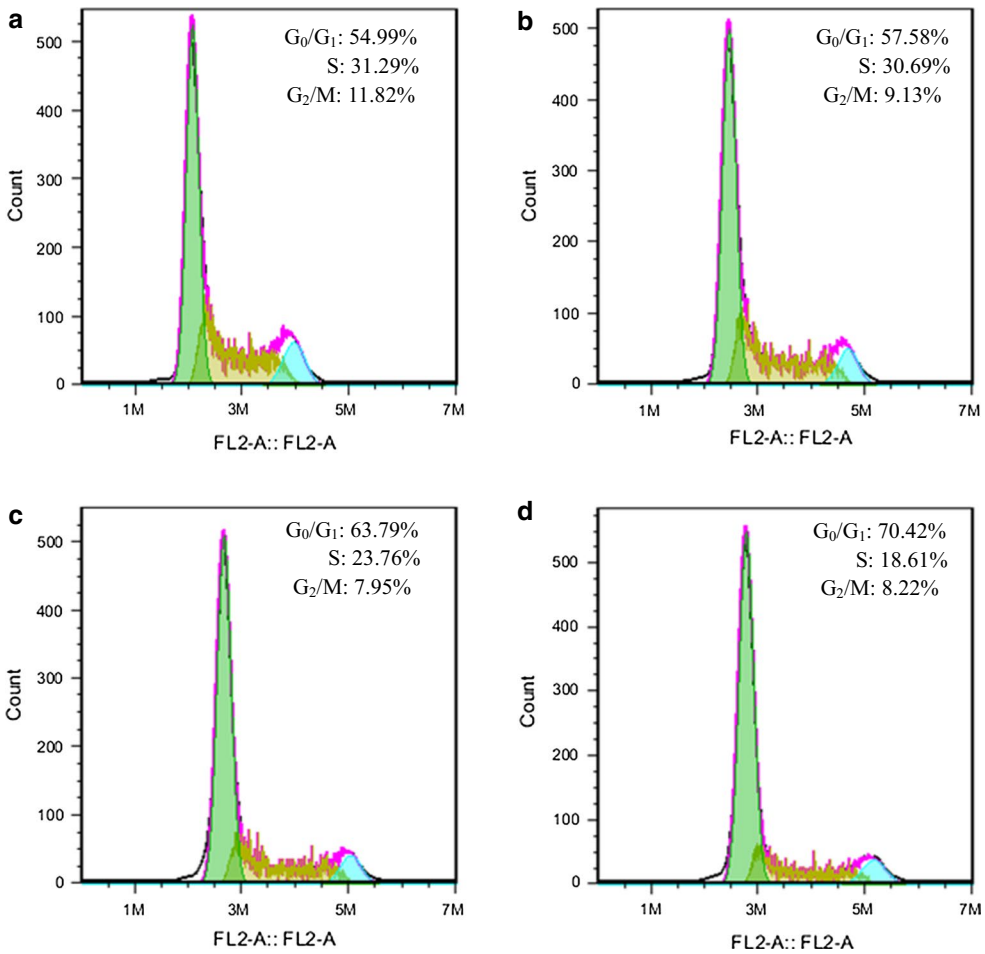


**Fig. 6** DNA content and cell cycle analysis of Hela cells after complex **1** treatment. Hela cells were cultured with complex **1** (**a** 0.1% DMSO (control); **b** 0.5 μM; **c** 1 μM; **d** 2 μM) for 24 h. The percentage of non-apoptotic cells within each cell cycle was determined by flow cytometry

progression, apoptosis, differentiation and evasion from cell death [48–50]. Because of its important role, the ERK signaling pathway has been the subject of intense research leading to the discovery and development of pharmacologic inhibitors for the treatment of cancer [45–48]. So it is worth noting that vanadium species have been closely linked with deregulation of cellular pathways through tyrosine phosphorylation. The Western blot analysis also showed that complex **1** attenuated the phosphorylation of ERK1/2 in Hela cells, similar to the U0126 (ERK pathway inhibitor), while having no effect on the total ERK1/2 levels. In conclusion, our study demonstrated that complex **1** inhibits cell proliferation by inducing apoptosis and $G_0/G_1$ phase arrest, and inhibition of the ERK1/2 signaling pathway may also contribute to the antitumor effects of these complexes.

## Experimental

### Materials and methods

$VO(acac)_2$ (acac = acetylacetonate) and 1,10-phenanthroline were purchased from Shanghai Jingchun company. Calf-thymus DNA (CT-DNA) and pBR 322 DNA were obtained from Sigma. Other materials were obtained from commercial sources and used as received (analytical reagents). Tris–HCl buffer A (5 mM Tris(hydroxymetylaminomethane)–HCl, 50 mM NaCl, pH = 7.2) was used for absorption titrations, luminescence titrations, and viscosity experiments. Tris–HCl buffer B (50 mM Tris–HCl and 18 mM NaCl, pH = 7.2) was used for DNA cleavage experiments. All buffers were prepared using double-distilled water. A solution of CT-DNA in the buffer gave a ratio of UV absorbance at 260 and 280 nm of ca. 1.8–1.9, indicating that the DNA was sufficiently free of protein [31]. The DNA concentration per nucleotide was determined by absorption spectroscopy using the molar absorption coefficient (6600 $M^{-1}$ $cm^{-1}$) at 260 nm [32]. Hela, BIU-87 and SPC-A-1 cell lines were purchased from The Cell Bank of Type Culture Collection of the Chinese Academy of Sciences (Shanghai, China). RPMI 1640 medium was purchased from Hyclone (Logan, USA); trypsin, fetal calf serum and Annexin V-FITC/PI apoptosis detection Kit were purchased from GIBCO company (USA). Hoechst 33258 staining solution was purchased from Beyotime Institute of Biotechnology (China). MTT, rhodamine

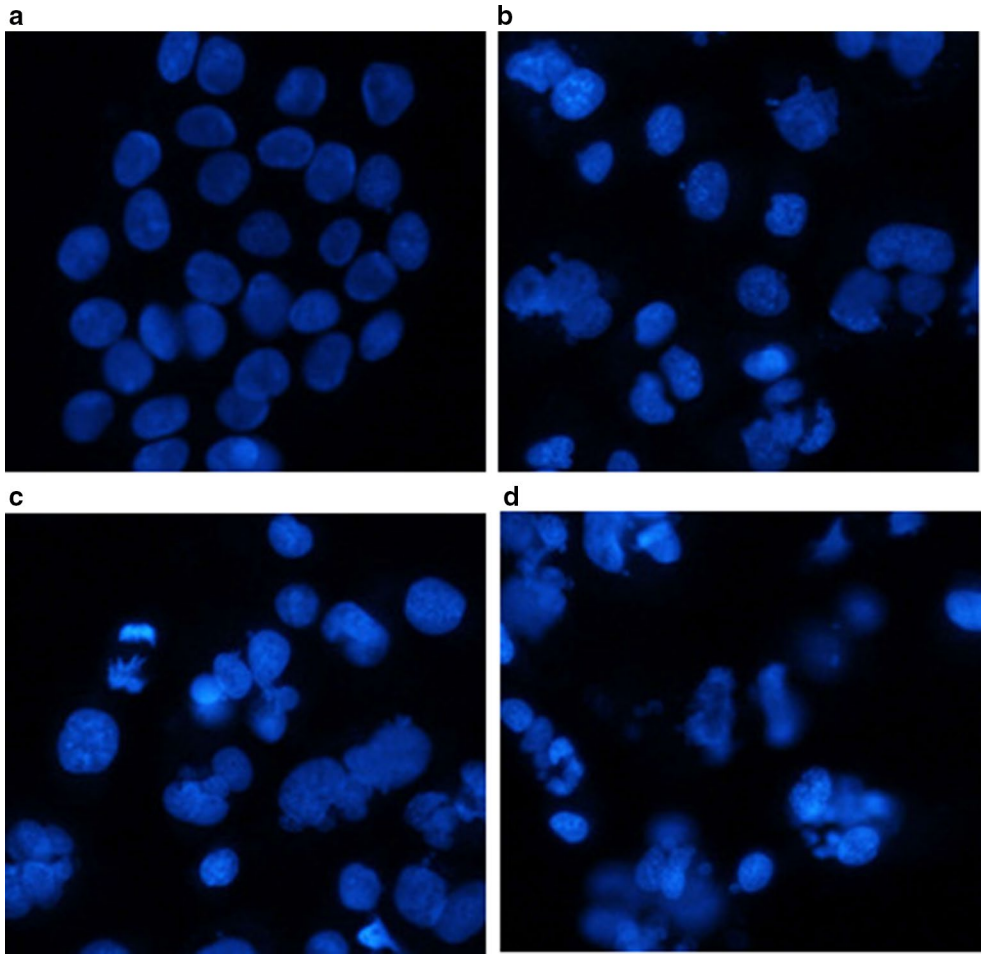


**Fig. 7** Effects of complex **1** on the morphology of Hela cells were assayed by Hoechst 33258 staining. After treatment with complex **1** [**a** 0.1% DMSO (control); **b** 0.5 μM; **c** 1 μM; **d** 2 μM] for 24 h, apoptotic cells were detected by Hoechst 33258 staining and examined by fluorescence microscopy

123 and U0126 (ERK1/2 inhibitor) were purchased from Sigma (USA). Anti-p-ERK1/2, anti-ERK1/2 and β-actin antibodies were purchased from Santa Cruz Biotechnology (USA).

Microanalyses (C, H, S and N) were obtained out with a PerkinElmer 240Q elemental analyzer. Electrospray mass spectra (ES-MS) were recorded on an LCQ system (Finnigan MAT, USA) using methanol as mobile phase. Infrared spectra were recorded on a PerkinElmer Lambda 35 instrument using KBr pellets. $^{1}$H and $^{13}$C-NMR spectra were recorded on a Varian-500 spectrometer. All chemical shifts are given relative to tetramethylsilane (TMS). UV–Vis spectra were recorded on a Shimadzu UV-3101 PC spectrophotometer at room temperature. Emission spectra were recorded on a PerkinElmer Lambda 55 spectrofluorophotometer. Molar conductivities in DMF (1 mM/l) solution at room temperature were measured using a DDS-307 digital direct reading conductivity meter. Cell cycle analysis and Annexin V-FITC/PI assay of apoptotic cells were recorded on a FACScan flow cytometer (BD FACSCalibur™, USA). Fluorescence microscopy of apoptosis assays was carried out with a fluorescence microscope (Olympus OX31, Olympus Corporation, Japan).

## DNA binding and cleavage

Absorption titration experiments were performed with fixed concentration of the complexes (20 μM), while gradually increasing the concentration of CT-DNA. V-DNA solutions were allowed to incubate for 5 min before the absorption spectra were recorded. In order to compare the binding strength of the complexes, their intrinsic binding constants ($K_b$) were determined by monitoring the changes of absorbance in the ligand transfer band with increasing concentration of CT-DNA. $K_b$ was then calculated using the following equation [33–41]:

$$\frac{[\mathrm{DNA}]}{\varepsilon_a - \varepsilon_f} = \frac{[\mathrm{DNA}]}{\varepsilon_b - \varepsilon_f} + \frac{1}{K_b(\varepsilon_b - \varepsilon_f)}$$

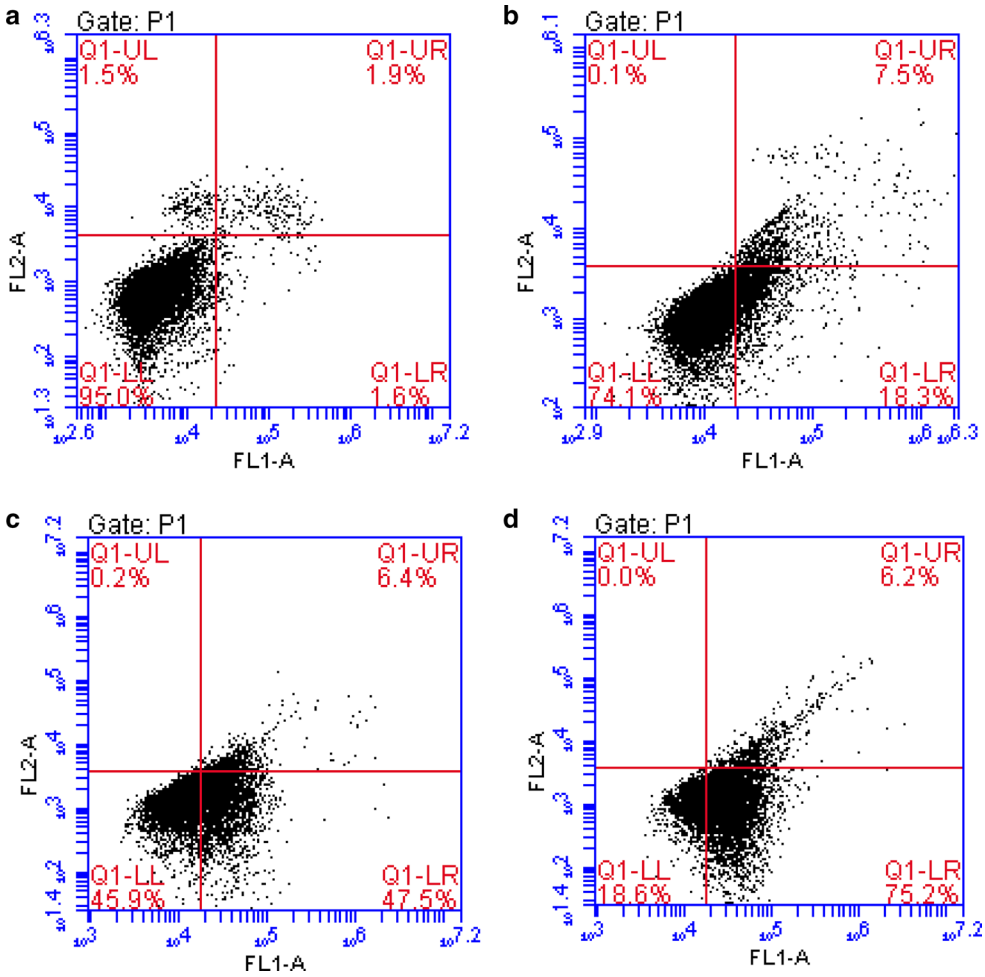


**Fig. 8** Distribution map of cell apoptosis. Hela cells were incubated with different concentrations of the complex 1 [**a** 0.1% DMSO (control); **b** 0.5 μM; **c** 1 μM; **d** 2 μM] for 24 h, and subjected to Annexin V-FITC/PI staining, and analyzed by flow cytometry

where [DNA] is the concentration of DNA in the base pairs, $\varepsilon_a$ is the extinction coefficient observed for $A_{obsed}/[V]$, $\varepsilon_b$ is the extinction coefficient of the complex when fully bound to DNA and $\varepsilon_f$ is the extinction coefficient of the complex in free solution.

Viscosity measurements were taken with an Ubbelohde viscometer maintained at a constant temperature of (28.0 ± 0.1) °C in a thermostatic bath. A digital stopwatch was used for flow time, and each sample was measured five times to obtain the average flow time. Data are presented as $(\eta/\eta_0)^{1/3}$ versus binding ratio [42], where $\eta$ is the viscosity of DNA in the presence of the complex and $\eta_0$ is the viscosity of DNA alone [41].

The cleavage of supercoiled pBR322 DNA by the complexes was studied by gel electrophoresis; pBR322 DNA (0.1 μg) was treated with the required complex in buffer B, and the solution was incubated at 37 °C. The samples were analyzed by electrophoresis for 1.5 h at 85 V on a 0.8% agarose gel in TBE (89 mM Tris–borate acid, 2 mM EDTA, pH = 8.3). The gel was stained with 1 μg/ml ethidium bromide and photographed on an Alpha Innotech IS-5500 fluorescence chemiluminescence and visible imaging system [18].

## Cytotoxicity assays

The effects of the test compounds on the growth of Hela, BIU-87 and SPC-A-1 cell lines were determined with the aid of MTT dye assays. The compounds were dissolved in DMSO (0.1%) and diluted with RPMI 1640 to the required concentrations prior to use. The control was prepared by addition of culture medium (100 μL). Wells containing culture medium without cells were used as blanks. Hela, BIU-87 and SPC-A-1 with a density $2 \times 10^4$ cells per well were precultured in 96-well microtiter plates for 48 h at 37 °C, 5% $CO_2$. Upon completion of the incubation, stock MTT dye solution was added to each well. After 4 h incubation, a solution containing *N*,*N*-dimethylformamide (50%) plus sodium dodecyl sulfate (20%) was added to solubilize the MTT formazan. The cell viability was determined by measuring the absorbance of each well at 490 nm using a Multiskan ASCENT microplate reader. $IC_{50}$ values were determined by

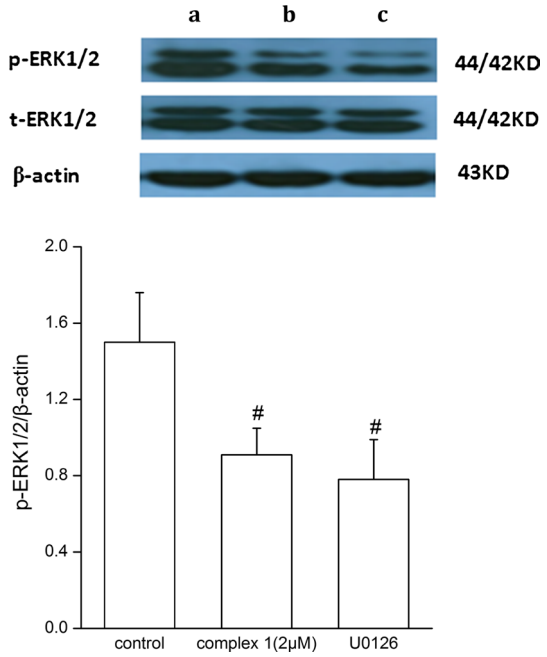


**Fig. 9** Complex **1** attenuated the phosphorylation of ERK1/2. a: control; b: complex **1** (2 μM); c:U0126. Hela cells treated with the complex **1** (2 μM) or U0126 (ERK pathway inhibitor) for 24 h. All data were presented as mean ± SE. #$P < 0.05$, versus control

plotting the percentage viability versus concentration on a logarithmic graph and reading off the concentration at which 50% of cells remained viable relative to the control [29, 30].

## Cell cycle analysis

Analysis of the cell cycle of both control and treated cancer cells was determined. Using standard methods, the DNA of cells was stained with PI, and the proportions of non-apoptotic cells in different phases of the cell cycle were recorded. The cancer cells were treated with the complexes, harvested by centrifugation at 1000*g* for 5 min, and then washed with ice-cold PBS. The collected cells were fixed overnight with cold 70% ethanol and then stained with PI solution consisting of 50 μg/ml PI plus 10 μg/ml RNase. After incubating for 10 min at room temperature in the dark, fluorescence-activated cells were sorted with a FACScan flow cytometer using CellQuest 3.0.1 software.

## Fluorescence microscopy of apoptosis assays

This method was modified from a previous report [43]. Briefly, after exposure to the complexes for 24 h, Hela cells were washed twice with PBS and then stained with 10 μg/ml Hoechst 33258 staining solution at 37 °C for 30 min according to the manufacturer's instructions. Finally, the cells were observed under a fluorescence microscope.

## Annexin V-FITC/PI assay of apoptotic cells

Hela cells treated with the complexes for 24 h were determined by flow cytometry using a commercially available Annexin V-FITC/PI apoptosis detection kit. After treatment, cells were harvested, washed twice in ice-cold PBS, and resuspended in 500 μl of binding buffer at 1–5 × $10^5$ cells/ml. The samples were incubated with 5 μl of Annexin V-FITC and 5 μl propidium iodide in the dark for 15 min at room temperature. Finally, samples were analyzed by flow cytometry and evaluated based on the percentage of cells for Annexin V positive.

## Western blot analysis

The ERK1/2 phosphorylation assay was performed as previously described [44]. The total proteins were extracted from cultured Hela cells treated with complex **1** (2 μM) or U0126 (ERK pathway inhibitor) for 24 h. Western blots were performed according to the manufacturer's procedures. Equal samples from each group were separated by SDS polyacrylamide gel electrophoresis for 1 h and transferred onto a PVDF membrane. The membranes were blocked in 5% BSA for 1 h at room temperature and then incubated with primary antibody (p-ERK1/2, t-ERK1/2, β-actin) overnight at 4 °C, followed by secondary antibody conjugation to horseradish peroxidase for 2 h. Immunoblots were visualized with ECL Western-blotting detection reagents and analyzed with Image pro plus V7.0 software.

## Synthesis of 2-(4-nitrophenyl)-imidazo[4,5-f]1,10-phenanthroline (NPIP)

A solution of phenanthraquinone (2.5 mmol, 0.45 g), ammonium acetate (50 mmol, 3.85 g) and p-nitrobenzaldehyde (3.5 mmol, 0.53 g) in glacial acetic acid 10 ml was refluxed for 6 h. The cooled deep red solution was diluted with water (25 ml) and neutralized with ammonium hydroxide. The mixture was filtered, and the precipitate was washed with water. The crude product was purified by chromatography over 60–80 mesh $SiO_2$ using absolute ethanol as eluent. The solvent was removed, and the product was collected and dried at 50 °C in vacuo. Yield: 88%. Anal. Calcd.: C, 66.86; H, 3.25; N, 20.52%; Found: C, 66.64; H, 3.33; N, 20.47%. ES-MS ($CH_3OH$, *m*/*z*): 342.0 ($[M + 1]^+$). IR (KBr) ($\nu_{max}$/$cm^{-1}$): 3096 s, 1601 m, 1564 m, 1516 s, 1476 s, 1455 s, 1421 s, 1397 s, 1344 s, 1296 m, 1109 m, 857 m, 806 m, 739 s, 707 m, 617 m. $^1$H-NMR (500 MHz, DMSO-d6): 9.02 (*d*, 2H), 8.85 (*d*, 2H), 8.45 (*d*, 2H), 8.40 (*d*, 2H), 7.80 (*q*, 2H).$^{13}$C-NMR

(600 MHz, DMSO-d6): 172.17, 148.33, 147.07, 147.28, 143.86, 135.93, 129.71, 126.83, 124.30, 123.30.

### Synthesis of 2-(4-chlorphenyl)-imidazo[4,5-f]1,10-phenanthroline) (CPIP)

**CPIP** was synthesized by a similar procedure as for NPIP, but with p-chlorobenzaldehyde (3.5 mmol, 0.49 g) in place of p-nitrobenzaldehyde. Yield: 80%. Anal. Calcd.: C, 68.99; H, 3.35; N, 16.94%; Found: C, 68.87; H, 3.42; N, 16.94%. ES-MS ($CH_3OH$, *m/z*): 331.1($[M + 1]^+$). IR (KBr) ($\nu_{max}$/$cm^{-1}$): 3079 s, 1686 m, 1604 m, 1563 m, 1514 m, 1475 s, 1451 s, 1420 m, 1397 m, 1352 m, 1191 m, 1102 m, 1071 m, 1014 m, 955 m, 836 m, 803 m, 738 s, 704 m, 687 m, 547 m. $^1$H NMR (500 MHz, DMSO-d6):9.04 (*d*, 2H), 8.90 (*d*, 2H), 8.50 (*d*, 2H), 8.45 (*d*, 2H), 7.84 (*q*, 2H). $^{13}$C-NMR (500 MHz, DMSO-d6, ppm): 149.44, 147.88, 143.13, 129.59, 129.12, 128.91, 127.85, 123.29.

### Synthesis of 2-(4-methylphenyl)-imidazo[4,5-f]1,10-phenanthroline) (MEPIP)

**MEPIP** was synthesized by a similar procedure as for NPIP but with p-methyl benzaldehyde (3.5 mmol, 0.42 g) in place of p-nitrobenzaldehyde. Yield: 83%. Anal. Calcd.: C, 73.61; H, 4.32; N, 17.17%; Found: C, 73.57; H, 4.38; N, 17.11%. ES-MS ($CH_3OH$, *m/z*): 327.1($[M + 1]^+$). IR (KBr) ($\nu_{max}$/$cm^{-1}$):3081 s, 1612 m, 1561 s, 1523 m, 1483 s, 1453 m, 1397 m, 1353 m, 1189 m, 1070 m, 1030 m, 957 m, 824 m, 803 m, 739 s, 723 m, 687 m, 646 m. $^1$H NMR (500 MHz, DMSO-d6): 9.05 (*d*, 2H), 8.94 (*d*, 2H), 8.19 (*d*, 2H), 7.84 (*q*, 2H), 7.44 (*d*, 2H), 1.913 (*s*, 3H). $^{13}$C NMR (500 MHz, DMSO-d6, ppm): 172.05, 150.72, 147.74, 143.55, 139.31, 129.58, 127.32, 123.26, 21.01.

### Synthesis of 2-(4-hydroxylphenyl)-imidazo[4,5-f] 1,10-phenanthroline) (HPIP)

**HPIP** was synthesized by a similar procedure as for NPIP but with p-hydroxybenzaldehyde (3.5 mmol, 0.48 g) in place of p-nitrobenzaldehyde. Yield: 80%. Anal. Calcd.: C, 73.07; H, 3.87; N, 17.94%; Found: C, 72.97; H, 3.95; N, 17.86%. ES-MS ($CH_3OH$, *m/z*): 313.0 ($[M + 1]^+$). IR (KBr)($\nu_{max}$/$cm^{-1}$): 3396 m, 3160 s, 1614 s, 1593 m, 1566 m, 1522 m, 1482 s, 1455 m, 1419 m, 1401 m, 1355 m, 1279 m, 1231 m, 1184 m, 1073 m, 1032 m, 960 m, 835 m, 801 m, 738 s, 692 m. $^1$H NMR (500 MHz, DMSO-d6):9.04 (*d*, 2H), 8.92 (*d*, 2H), 8.32 (*d*, 2H), 7.84 (*d*, 2H), 7.47 (*d*, 2H), 3.28 (*s*, H). $^{13}$C NMR (500 MHz, DMSO-d6, ppm): 150.63, 147.68, 142.87, 129.66, 128.12, 123.28.

### Synthesis of 2-hydroxy-1-naphthaldehyde thiosemicarbazone (hntdtsc)

A solution of 2-hydroxy-1-naphthaldehyde (5 mmol, 0.86 g) in absolute ethanol (10 ml) was added dropwise to a stirred solution of thiosemicarbazide (5 mmol, 0.455 g) in absolute ethanol (10 ml). The mixture was stirred at 50 °C for 3 h to give a white precipitate, which was used without further purification. Yield: 1.03 g, 84%. Anal. Calcd.: C, 58.76; H, 4.52; N, 17.13; S, 13.07%; Found: C, 58.70; H, 4.61; N, 17.08; S, 13.01%. ES-MS ($CH_3OH$, *m/z*): 246.0 ($[M + 1]^+$). IR (KBr) ($\nu_{max}$/$cm^{-1}$): 3450 s, 3253 s, 3167 m, 3053 m, 1625 s, 1593 m,1572 s, 1509 m, 1472 m, 1452 m, 1033 m, 1240 m, 821 m, 753 m. $^1$H NMR (500 MHz, DMSO-d6): 11.42 (*s*, 1H), 10.51 (*s*, 1H), 9.06 (*s*, 1H), 7.85 and 8.25 (2br *s*, 1H), 8.53 (*d*, 1H), 7.89 (*d*, 1H), 7.86 (*d*, 1H), 7.57 (*t*, 1H),7.38 (*t*, 1H), 7.21 (*d*, 1H). $^{13}$C NMR (500 MHz, DMSO-d6, ppm): 156.61, 143.03, 132.48, 131.51, 128.68, 128.06, 127.88, 123.45, 122.86, 118.33, 109.76.

### Synthesis of [VO(hntdtsc)(NPIP)] (1)

A mixture of hntdtsc (0.5 mmol, 0.123 g) and NPIP (0.5 mmol, 0.171 g) in absolute methanol (100 ml) was heated at 80 °C under argon for 2 h. After dissolution, a solution of $VO(acac)_2$ (0.5 mmol, 0.132 g) methanol (10 ml) was added dropwise to this mixture. The mixture was refluxed for another 4 h to give a reddish-brown precipitate. The solid powder was isolated from the hot solution, washed with absolute methanol and dried in vacuo. Yield: 76%. Anal. Calcd.: C, 57.15; H, 3.09; N, 17.20; S, 4.92%; Found: C, 57.09; H, 3.14; N, 17.16; S, 4.89%. ES-MS ($CH_3OH$, *m/z*): 652.1 ($[M + 1]^+$). IR (KBr) ($\nu_{max}$/$cm^{-1}$): 3355 m. 3180 m. 1615 m, 1599 s, 1538 m, 1514 s, 1454 m, 1340 s, 1193 m, 955 m, 856 m, 825 m, 731 m, 709 m, 498 m. $^1$H NMR (500 MHz, DMSO-d6): 9.39 (*s*, H),9.04 (*d*, 2H),8.88 (*m*, 2H),8.49 (br *s*, 3H), 8.19 (*s*, 1H),7.82 (*m*, 3H), 7.56 (br *m*, 1H), 7.37 (br *m*, 1H), 7.31 (*s*, 1H), 7.19 (*d*, 2H), 7.09 (*d*, 2H), 6.66 (*s*, H).

### Synthesis of [VO(hntdtsc)(CPIP)] (2)

Complex **2** was synthesized by a similar procedure as for complex **1**, but with CPIP (0.5 mmol, 0.166 g) in place of NPIP. Yield: 70%. Anal. Calcd.: C, 58.09; H, 3.14; N, 15.30; S, 5.00%; Found: C, 57.97; H, 3.23; N, 15.22; S, 4.82%. ES-MS ($CH_3OH$, *m/z*): *639.1*($[M + 1]^+$). IR (KBr) ($\nu_{max}$/$cm^{-1}$): 3318 m, 3175 m, 1615 m, 1598 s, 1575 m, 1538 s, 1504 s, 1454 s, 1427 m, 1334 m, 1193 m, 945 m, 821 m, 738 m, 730 m, 498 m. $^1$H NMR (500 MHz, DMSO-$d_6$): 9.36 (*s*, H), 9.04 (*d*, 2H), 8.89 (*m*, 2H), 8.52 (br *m*, 3H), 8.28 (br s,1H), 7.71-7.82(*d*, 3H), 7.56 (br *m*, 1H), 7.38 (br *m*, 1H), 7.326 (*s*, 1H), 7.20 (*d*, 2H), 7.01 (*d*, 2H), 6.649 (*s*, H).

### Synthesis of [VO(hntdtsc)(MEPIP)] (3)

Complex **3** was synthesized by a similar procedure as for complex **1**, but with MEPIP (0.5 mmol, 0.164 g) in place of NPIP. Yield: 67%. Anal. Calcd.: C, 61.39; H, 3.74; N, 15.80; S, 5.17%; Found: C, 61.33; H, 3.86; N, 15.73; S, 5.14. %. ES-MS ($CH_3OH$, *m/z*): 619.1 ($[M + 1]^+$). IR (KBr) ($\nu_{max}/cm^{-1}$): 3367 m, 1614 s, 1598 s, 1575 m, 1538 s, 1504 m, 1482 s, 1454 m, 1427 m, 1399 m, 1362 m, 1337 m, 1191 m, 1077 m, 961 m, 824 m, 737 m, 499 m, 427 m. $^1$H NMR (500 MHz, DMSO-d6): 9.39 (*s*, H), 9.04 (*d*, 2H), 8.92 (*m*, 2H), 8.51 (br *m*, 3H), 8.43 (br s,1H), 7.83(*d*, 3H), 7.55 (br *m*, 1H), 7.38-7.43 (br *m*, 3H), 7.21 (*s*, 1H), 7.20 (*d*, 2H), 6.99 (*d*, 2H), 6.61 (*s*, H),2.14 (*s*, 3H).

### Synthesis of [VO(hntdtsc)(HPIP)] (4)

Complex **4** was synthesized by a similar procedure as for complex **1**, but with HPIP (0.5 mmol, 0.156 g) in place of NPIP. Yield: 72%. Anal. Calcd.: C, 59.81; H, 3.40; N, 15.75; S, 5.15%; Found: C, 59.71; H, 3.53; N, 15.69; S, 5.09%. ES-MS ($CH_3OH$, *m/z*): 623.0($[M + 1]^+$). IR (KBr) ($\nu_{max}/cm^{-1}$): 3320 m, 3191 m, 1614 s, 1597 s, 1597 m, 1575 m, 1537 m, 1482 s, 1454 m, 1428 m, 1386 m, 1362 m, 1336 m, 1278 m, 1247 m, 1176 m, 1193 m, 1079 m, 947 m, 824 m, 742 m, 730 m, 499 m. $^1$H NMR (500 MHz, DMSO-$d_6$): 9.40 (*s*, H), 9.05 (*d*, 2H), 8.95 (*d*, 2H), 8.50 (br *m*, 3H), 8.40 (br *s*, 1H), 7.83(*d*, 3H), 7.55 (br *m*, 1H), 7.38-7.43 (br *m*, 3H), 7.18-32 (br *m*, 2H), 6.94-7.00 (br *m*, 2H),3.17 (*s*, 1H).

**Acknowledgements** This study was supported by Natural Science Foundation of Gansu Province, China (Grant No. 145RJZA143) and Administration of traditional Chinese medicine Scientific Research Funds of Gansu Province (Grant No. GZK-2017-53). We thank Dr. Zhi-Jian Han for language editing and improvement.

**Conflict of interest** The authors declare that they have no conflict of interest.

## References

1. Leon IE, Cadavid-Vargas JF, Di Virgilio AL, Etcheverry S (2017) Vanadium, ruthenium and copper compounds: a new class of non-platinum metallodrugs with anticancer activity. Curr Med Chem 24(2):112–148
2. Sanna D, Ugone V, Fadda A, Micera G, Garribba E (2016) Behavior of the potential antitumor V(IV)O complexes formed by flavonoid ligands. 3. Antioxidant properties and radical production capability. J Inorg Biochem 161:18–26
3. Andrezalova L, Gbelcova H, Durackova Z (2013) DNA damage induction and antiproliferative activity of vanadium(V) oxido monoperoxido complex containing two bidentate heteroligands. J Trace Elem Med Biol 27:21–26
4. Wang G, Wang J, Fu Y, Bai L, He M, Li B, Fu Q (2013) Systemic treatment with vanadium absorbed by *Coprinus comatus* promotes femoral fracture healing in streptozotocin-diabetic rats. Biol Trace Elem Res 151:424–433
5. Reddy GNR, Kondaiah S, Setty KN, Rao RM, Ramulu JS (2012) Synthesis, structural characterization and anti-bacterial activity of some novel Schiff base ligands and their vanadium(IV) metal complexes. Orient J Chem 28(4):1673–1683
6. Park S-J, Youn C-K, Hyun JW, You HJ (2013) The anti-obesity effect of natural vanadium-containing Jeju ground water. Biol Trace Elem Res 151(2):294–300
7. Holko P, Ligeza J, Kisielewska J, Kordowiak AM, Klein A (2008) The effect of vanadyl sulphate ($VOSO_4$) on autocrine growth of human epithelial cancer cell lines. Pol J Pathol 59:3–8
8. Klein A, Holko P, Ligeza J, Kordowiak AM (2008) Sodium orthovanadate affects growth of some human epithelial cancer cells (A549, HTB44, DU145). Folia Biol (Krakow) 56:115–121
9. Molinuevo MS, Cortizo AM, Etcheverry SB (2008) Vanadium(IV) complexes inhibit adhesion, migration and colony formation of UMR106 osteosarcoma cells. Cancer Chemother Pharmacol 61:767–773
10. Rodríguez-Mercado JJ, Mateos-Nava RA, Altamirano-Lozano MA (2011) DNA damage induction in human cells exposed to vanadium oxides in vitro. Toxicol In Vitro 25:1996–2002
11. Soares SS, Henao F, Aureliano M, Gutiérrez-Merino C (2008) Vana-date induces necrotic death in neonatal rat cardiomyocytes through mitochondrial membrane depolarization. Chem Res Toxicol 21:607–618
12. Zhao Y, Ye L, Liu H, Xia Q, Zhang Y, Yang X, Wang K (2010) Vanadium compounds induced mitochondria permeability transition pore (PTP) opening related to oxidative stress. J Inorg Biochem 104:371–378
13. Pessoa JC, Etcheverry SB, Gambino D (2015) Vanadium compounds in medicine. Coord Chem Rev 301:24–48
14. Ying P, Zeng P, Jiazheng L, Chen H, Liao X, Yang N (2015) New oxidovanadium complexes incorporating thiosemicarbazones and 1, 10-phenanthroline derivatives as DNA cleavage, potential anticancer agents, and hydroxyl radical scavenger. Chem Biol Drug Des 86:926–937
15. Hwang JH, Larson RK, Abu-Omar MM (2003) Kinetics and mechanistic studies of anticarcinogenic bisperoxovanadium(V) compounds: ligand substitution reactions at physiological pH and relevance to DNA interactions. Inorg Chem 42(24):7967–7977
16. Wu H-L, Li K, Sun T, Kou F, Jia F, Yuan J-K, Liu B, Qi B-L (2011) Synthesis, structure, and DNA-binding properties of manganese(II) and zinc(II) complexes with tris(*N*-methylbenzimidazol-2-ylmethyl)amine ligand. Transition Met Chem 36(1):21–28
17. Ji LN, Zhou XH, Liu JG (2001) DNA-binding activities and potential antitumor properties of some ruthenium complexes. Coord Chem Rev 216–217(1):513–516
18. Leelavathy L, Anbu S, Kandaswamy M et al (2009) Antibacterium properties of some porphyrin derivatives. Polyhedron 28(2):903–910
19. Fiel RJ, Munson BR (1980) Binding of meso-tetra(4-*N*-methylpyridyl)porphine to DNA. Nucleic Acids Res 8(12):2835–2842
20. Pasternack RF, Gibbs EJ, Villafranca JJ (1983) Possible mechanism of potential anticancer properties of some ruthenium complexes. Biochemistry 22(2):2406–2414
21. Satyanarayana S, Dabrowiak JC, Chaires JB (1992) Synthesis, characterization and DNA-binding activities of porphyrins. J Biochem 31(4):9319–9324
22. Uno T, Hamasaki K, Tanigawa M, Shimabayashi S (1997) Binding of meso-tetrakis(*N*-methylpyridinium-4-yl)porphyrin to double helical RNA and DNA–RNA Hybrids. Inorg Chem 36(8):1676–1683

23. Kovala-Demertzi D, Demertzis MA, Miller JR, Papadopoulou C, Dodorou C, Filousis G (2001) Platinum(II) complexes with 2-acetylpyridine thiosemicarbazone. Synthesis, crystal structure, spectral properties, antimicrobial and antitumour activity. J Inorg Biochem 86(2–3):555–563
24. McGhee JD (1976) Theoretical calculations of the helix-coil transition of DNA in the presence of large, cooperatively binding ligands. Biopolymers 15(7):1345–1375
25. Waring MJ (1965) Complex formation between ethidium bromide and nucleic acids. J Mol Biol 13(1):269–282
26. Barton JK, Raphael AL (1984) Photoactivated stereospecific cleavage of double-helical DNA by cobalt(III) complexes. J Am Chem Soc 106(8):2466–2468
27. Zhang Q-L, Liu J-G, Liu J-Z, Li H, Yang Y, Xu H, Chao H, Ji L-N (2002) Effect of intramolecular hydrogen-bond on the DNA-binding and photocleavage properties of polypyridyl cobalt(III) complexes. Inorg Chim Acta 339:34–40
28. Brooks HB, Sicilio F (1971) Electron spin resonance kinetic studies of the oxidation of vanadium(IV) by hydrogen peroxide. Inorg Chem 10(11):2530–2534
29. Vermes I, Haanen C, Steffens-Nakken H, Reutelingsperger C (1995) J Immunol Methods 184:39–51
30. Kim R (2005) Recent advances in understanding the cell death pathways activated by anticancer therapy. Cancer 103(8):1551–1560
31. Marmur J (1961) A procedure for the isolation of deoxyribonucleic acid from micro.ovrddot.organisms. J Mol Biol 3:208
32. Cohen G, Eisenberg H (1969) Viscosity and sedimentation study of sonicated DNA-proflavine complexes. Biopolymers 8(1):45–55
33. Benitez J, Becco L, Correia I, Leal SM, Guiset H, Pessoa JC, Lorenzo J, Tanco S, Escobar P, Moreno V, Garat B, Gambino D (2011) Vanadium polypyridyl compounds as potential antiparasitic and antitumoral agents: new achievements. J Inorg Biochem 105(2):303–312
34. Liang X-L, Tan L-F, Zhu W-G (2011) Study on DNA-binding and DNA-cleavage properties of Cr(III) complexes with polypyridyl ligands. DNA Cell Biol 30(1):61–67
35. Zhao P, Lian-Cai X, Huang J-W, Bo F, Han-Cheng Yu, Ji L-N (2008) Tricationic pyridium porphyrins appending different peripheral substituents: experimental and DFT studies on their interactions with DNA. Biophys Chem 135:102–109
36. Zhao P, Lian-Cai X, Huang J-W, Bo F, Han-Cheng Yu, Ji L-N (2008) Experimental and DFT studies on DNA binding and photocleavage of two cationic porphyrins: Effects of the introduction of a carboxyphenyl into pyridinium porphyrin. Spectrochim Acta Part A Mol Biomol Spectrosc 71:1216–1223
37. Zhao P, Lian-Cai X, Huang J-W, Bo F, Han-Cheng Yu, Ji L-N (2008) DNA binding and photocleavage properties of cationic porphyrin-anthraquinone hybrids with different lengths of links. Bioorg Chem 36:278–287
38. Kurita N, Kobayashi K (2000) Comput Chem 24:351–355
39. Jia-Zheng L, Yi-Fan D, Guo H-W (2011) Two oxovanadium complexes incorporating thiosemicarbazones: synthesis, characterization and DNA-binding studies. J Coord Chem 64(7):1229–1239
40. Du YF, Lu JZ, Guo HW et al (2010) Synthesis, characterization and photocleavage activities of oxovanadium complexes. Transit Metal Chem 35(7):859–864
41. Li C, Wu J, Wang L, Min R, Jia N, Guo J (1999) Synthesis, characterization and antitumor activity of copper(II) complex with nicotinamido-4-bis(2-chloroethyl)aminobenzaldimine. J Inorg Biochem 73(4):195–202
42. Liu YJ, Zeng CH, Huang HL et al (2010) DNA-binding, photocleavage and anticancer activities of some rhyseniuim complexes. J Eur Med Chem 45(12):564–571
43. Xu HL, Yu XF, Qu SC, Zhang R, Qu XR, Chen YP, Ma XY, Sui DY (2010) Anti-proliferative effect of Juglone from Juglans mandshurica Maxim on human leukemia cell HL-60 by inducing apoptosis through the mitochondria-dependent pathway. Eur J Pharmacol 645:14–22
44. Zhao Q, Bai Y, Li C et al (2017) Oleuropein protects cardiomyocyte against apoptosis via activating the reperfusion injury salvage kinase pathway in vitro. Evid Based Complement Alternat Med eCAM 2017:2109018
45. Roberts PJ, Der CJ (2007) Targeting the Raf-MEK-ERK mitogen-activated protein kinase cascade for the treatment of cancer. Oncogene 26(22):3291–3310
46. Montagut C, Settleman J (2009) Targeting the RAF-MEK-ERK pathway in cancer therapy. Cancer Lett 283(2):125
47. Thompson N, Lyons J (2005) Recent progress in targeting the Raf/MEK/ERK pathway with inhibitors in cancer drug discovery. Curr Opin Pharmacol 5(4):350
48. De Luca A, Maiello MR, D'Alessio A et al (2012) The RAS/RAF/MEK/ERK and the PI3K/AKT signalling pathways: role in cancer pathogenesis and implications for therapeutic approaches. Expert Opin Ther Targets 16(Suppl 2):S17
49. Saini KS, Loi S, De AE et al (2013) Targeting the PI3K/AKT/mTOR and Raf/MEK/ERK pathways in the treatment of breast cancer. Cancer Treat Rev 39(8):935–946
50. Santarpia L, Lippman SM, Elnaggar AK (2012) Targeting the MAPK–RAS–RAF signaling pathway in cancer therapy. Expert Opin Ther Targets 16(1):103–119